A measurement of $\sigma_{tot}(\gamma p)$ at $\sqrt{s} = 210$ GeV

ZEUS Collaboration

M. Derrick, D. Krakauer, S. Magill, B. Musgrave, J. Repond, K. Sugano[1], R. Stanek,
R.L. Talaga, J. Thron

Argonne National Laboratory, Argonne, IL, USA

F. Arzarello, R. Ayed[2], G. Barbagli[3], G. Bari, M. Basile, L. Bellagamba, D. Boscherini,
G. Bruni, P. Bruni, G. Cara Romeo, G. Castellini[4], M. Chiarini, L. Cifarelli, F. Cindolo,
F. Ciralli, A. Contin, S. D'Auria, C. Del Papa, F. Frasconi, P. Giusti, G. Iacobucci,
G. Laurenti, G. Levi, Q. Lin, B. Lisowski, G. Maccarrone, A. Margotti, T. Massam, R. Nania,
C. Nemoz, F. Palmonari, G. Sartorelli, R. Timellini, Y. Zamora Garcia[2], A. Zichichi

University of Bologna and INFN Bologna, Bologna, Italy

A. Bargende, F. Barreiro[5], J. Crittenden, H. Dabbous, K. Desch, B. Diekmann, M. Geerts,
G. Geitz, B. Gutjahr, H. Hartmann, J. Hartmann, D. Haun, K. Heinloth, E. Hilger,
H.-P. Jakob, S. Kramarczyk, M. Kückes, A. Mass, S. Mengel, J. Mollen, H. Müsch, E. Paul,
R. Schattevoy, B. Schneider[6], J.-L. Schneider, R. Wedemeyer

Physikalisches Institut der Universität Bonn, Bonn, FRG

A. Cassidy, D.G. Cussans, N. Dyce, H.F. Fawcett, B. Foster, R. Gilmore, G.P. Heath,
M. Lancaster, T.J. Llewellyn, J. Malos, C.J.S. Morgado, R.J. Tapper, S.S. Wilson

Bristol University, Bristol, UK

R.R. Rau

Brookhaven National Laboratory, Upton, NY, USA

A. Bernstein, A. Caldwell, I. Gialas, J.A. Parsons, S. Ritz, F. Sciulli[7], P.B. Straub, L. Wai,
S. Yang

Nevis Laboratories, Columbia University, Irvington on Hudson, NY, USA

T. Barillari, M. Schioppa, G. Susinno

Physics Department, Calabria University, and INFN, Cosenza, Italy

W. Burkot, J. Chwastowski[8], A. Dwuraźny, A. Eskreys, B. Nizioł, Z. Jakubowski[9],
K. Piotrzkowski, M. Zachara, L. Zawiejski

Institute of Nuclear Physics, Cracow, Poland

P. Borzemski, K. Eskreys, K. Jeleń, D. Kisielewska, T. Kowalski, J. Kulka, E. Rulikowska-Zarębska, L. Suszycki, J. Zając

Institut of Physics and Nuclear Techniques, Academy of Mining and Metallurgy, Cracow, Poland

T. Kędzierski, A. Kotański, M. Przybycień

Department of Physics, Jagellonian University, Cracow, Poland

L.A.T. Bauerdick, U. Behrens, J.K. Bienlein, C. Coldewey, A. Dannemann, K. Dierks[10], W. Dorth[10], G. Drews, P. Erhard[11], M. Flasiński[12], I. Fleck, A. Fürtjes, R. Gläser[13], P. Göttlicher, T. Haas, L. Hagge, W. Hain, D. Hasell, H. Hultschig, G. Jahnen[14], P. Joos, M. Kasemann, R. Klanner, W. Koch, U. Kötz, H. Kowalski, J. Labs, A. Ladage, B. Löhr, M. Löwe, D. Lüke, J. Mainusch, O. Manczak[15], M. Momayezi, S. Nickel, D. Notz, I. Park, K.-U. Pösnecker[16], M. Rohde, E. Ros[8], U. Schneekloth, J. Schroeder, W. Schulz, F. Selonke, E. Tscheslog[17], T. Tsurugai, F. Turkot[18], W. Vogel[19], T. Woeniger[20], G. Wolf, C. Youngman

Deutsches Elektronen-Synchrotron DESY, Hamburg, FRG

H.J. Grabosch, A. Leich, A. Meyer, C. Rethfeldt, S. Schlenstedt

Institut für Hochenergiephysik, DESY-Zeuthen, Zeuthen, FRG

R. Casalbuoni, S. De Curtis, D. Dominici, A. Francescato, M. Nuti, P. Pelfer,

University of Florence and INFN, Florence, Italy

G. Anzivino, R. Casaccia, I. Laakso[21], S. De Pasquale, S. Qian, L. Votano

INFN, Laboratori Nazionali di Frascati, Frascati, Italy

A. Bamberger, A. Freidhof, T. Poser, S. Söldner-Rembold, G. Theisen, T. Trefzger

Physikalisches Institut der Universität Freiburg, Freiburg, FRG

N.H. Brook, P.J. Bussey, A.T. Doyle, J.R. Forbes, V.A. Jamieson, C. Raine, D.H. Saxon

Department of Physics and Astronomy, University of Glasgow, Glasgow, UK

G. Gloth, U. Holm, H. Kammerlocher, B. Krebs, T. Neumann, K. Wick

I. Institute of Experimental Physics, Hamburg University, Hamburg, FRG

A. Hofmann[21], W. Kröger, J. Krüger, E. Lohrmann, J. Milewski[15], M. Nakahata, N. Pavel, G. Poelz, R. Salomon[22], A. Seidman[23], W. Schott, B.H. Wiik, F. Zetsche

II. Institute of Experimental Physics, Hamburg University, Hamburg, FRG

T.C. Bacon, I. Butterworth, C. Markou, D. McQuillan, D.B. Miller, M.M. Mobayyen, A. Prinias, A. Vorvolakos

High Energy Nuclear Physics Group, Imperial College London, London, UK

T. Bienz, H. Kreutzmann, U. Mallik, E. McCliment, M. Roco, M.Z. Wang

Physics and Astronomy Department, University of Iowa, Iowa City, USA

P. Cloth, D. Filges

Institut für Kernphysik, Forschungszentrum Jülich, Jülich, FRG

L. Chen, R. Imlay, S. Kartik, H.-J. Kim, R.R. McNeil, W. Metcalf

Department of Physics and Astronomy, Louisiana State University, Baton Rouge, LA, USA

G. Cases, L. Hervás[24], L. Labarga [24], J. del Peso, J. Roldán, J. Terrón, J.F. de Trocóniz[25]

Departamento de Física Teórica, Universidad Autónoma de Madrid, Madrid, Spain

F. Ikraiam, J.K. Mayer, G.R. Smith

Department of Physics, University of Manitoba, Winnipeg, Manitoba, Canada

F. Corriveau, D.J. Gilkinson, D.S. Hanna[7], L.W. Hung, J.W. Mitchell, P.M. Patel,
L.E. Sinclair, D.G. Stairs, R. Ullmann

Department of Physics, McGill University, Montreal, Quebec, Canada

G.L. Bashindzhagyan, P.F. Ermolov, Y.A. Golubkov, V.A. Kuzmin, E.N. Kuznetsov,
A.A. Savin, A.G. Voronin, N.P. Zotov

Institute of Nuclear Pysics, Moscow State University, Moscow, Russia

S. Bentvelsen, A. Dake, J. Engelen, P. de Jong, S.de Jong[8], M. de Kamps, P. Kooijman,
A. Kruse, H. van der Lugt, V. O'Dell, J. Straver[8], A. Tenner, H. Tiecke, H. Uijterwaal[26],
J. Vermeulen, L. Wiggers, E. de Wolf, R. van Woudenberg, R. Yoshida

NIKHEF, Amsterdam, The Netherlands

B. Bylsma, L.S. Durkin, C. Li, T.Y. Ling, K.W. McLean, W.N. Murray, S.K. Park,
T.A. Romanowski, R. Seidlein

Physics Department, Ohio State University, Columbus, OH, USA

G.A. Blair, J.M. Butterworth, A. Byrne, R.J. Cashmore, A.M. Cooper-Sarkar,
R.C.E. Devenish, D.M. Gingrich, P.M. Hallam-Baker[9], N. Harnew, T. Khatri, K.R. Long,
P. Luffman, I. McArthur, P. Morawitz, J. Nash, S.J.P. Smith[27], N.C. Roocroft, F.F. Wilson

Department of Physics, University of Oxford, Oxford, UK

G. Abbiendi, R. Brugnera, R. Carlin, F. Dal Corso, M. De Giorgi, U. Dosselli, C. Fanin,
F. Gasparini, S. Limentani, M. Morandin, M. Posocco, L. Stanco, R. Stroili, C. Voci

Dipartimento di Fisica dell' Universita and INFN, Padova, Italy

J.N. Lim, B.Y. Oh, J. Whitmore[28]

Department of Physics, Pennsylvania State University, University Park, PA, USA

467

M. Bonori, U. Contino, G. D'Agostini, M. Guida, M. Iori, S. Mari, G. Marini, M. Mattioli, D. Monaldi, A. Nigro

Dipartimento di Fisica, Università 'La Sapienza', Rome, Italy

J.C. Hart, N.A. McCubbin, T.P. Shah, T.L. Short

Rutherford Appleton Laboratory, Chilton, Didcot, Oxon, UK

E. Barberis, N. Cartiglia, C. Heusch, B. Hubbard, J. Leslie, J.S.T. Ng, K. O'Shaughnessy, H.F. Sadrozinski, A. Seiden

University of California, Santa Cruz, CA, USA

E. Badura, J. Biltzinger, H. Chaves, M. Rost, R.J. Seifert, A.H. Walenta, W. Weihs, G. Zech

Fachbereich Physik der Universität-Gesamthochschule Siegen, Siegen, FRG

S. Dagan, R. Heifetz, A. Levy, D. Zer-Zion

School of Physics, Tel-Aviv University, Tel Aviv, Israel

T. Hasegawa, M. Hazumi, T. Ishii, S. Kasai [29], M. Kuze, Y. Nagasawa, M. Nakao, H. Okuno, K. Tokushuku, T. Watanabe, S. Yamada

Institute for Nuclear Study, University of Tokyo, Tokyo, Japan

M. Chiba, R. Hamatsu, T. Hirose, S. Kitamura, S. Nagayama, Y. Nakamitsu

Department of Physics, Tokyo Metropolitan University, Tokyo, Japan

M. Arneodo, M. Costa, M.I. Ferrero, L. Lamberti, S. Maselli, C. Peroni, A. Solano A. Staiano

Dipartimento di Fisica Sperimentale, Universita di Torino, and INFN, Turin, Italy

M. Dardo

Facultá di Scienze MFN, Universita di Torino, Alessandria, Italy

D.C. Bailey, D. Bandyopadhyay, F. Benard, S. Bhadra, M. Brkic, B.D. Burow, F.S. Chlebana, M.B. Crombie, G.F. Hartner, G.M. Levman, J.F. Martin, R.S. Orr, J.D. Prentice, C.R. Sampson, G.G. Stairs, R.J. Teuscher, T.-S. Yoon

Department of Physics, University of Toronto, Toronto, Ontario, Canada

F.W. Bullock, C.D. Catterall, J.C. Giddings, T.W. Jones, A.M. Khan, J.B. Lane, P.L. Makkar, D. Shaw, J. Shulman

Physics and Astronomy Department, University College London, London, UK

K. Blankenship, J. Kochocki, B. Lu, L.W. Mo

Physics Department, Virginia Polytechnic Institute, Blacksburg, VA, USA

K. Charchuła, J. Ciborowski, J. Gajewski, G. Grzelak, M. Kasprzak, M. Krzyżanowski, K. Muchorowski, R.J. Nowak, J.M. Pawlak, K. Stojda, A. Stopczyński, R. Szwed, T. Tymieniecka [30], R. Walczak, A.K. Wróblewski, J.A. Zakrzewski, A.F. Żarnecki

Institute of Experimental Physics, Warsaw University, Warsaw, Poland

M. Adamus

Institute for Nuclear Studies, Warsaw, Poland

H. Abramowicz [15], Y. Eisenberg, C. Glasman, U. Karshon, A. Montag, D. Revel, E.E. Ronat [21], A. Shapira

Nuclear Physics Department, Weizmann Institute, Rehovot, Israel

I. Ali, B. Behrens, U. Camerini, S. Dasu, C. Fordham, C. Foudas, A. Goussiou, M. Lomperski, R.J. Loveless, P. Nylander, M. Ptacek, D.D. Reeder, W.H. Smith, S. Silverstein

Department of Physics, University of Wisconsin, Madison, WI, USA

W.R. Frisken, K.M. Furutani and Y. Iga

Department of Physics, York University, North York, Ontario, Canada

Received 23 September 1992

The total photoproduction cross section is determined from a measurement of electroproduction with the ZEUS detector at HERA. The Q^2 values of the virtual photons are in the range $10^{-7} < Q^2 < 2 \times 10^{-2}$ GeV^2. The γp total cross section in the γp centre of mass energy range 186–233 GeV is 154 ± 16 (stat.) ± 32 (syst.) μb.

1. Introduction

The total photon–proton cross section is predicted to rise substantially with increasing energy from its value of 118 μb at a centre of mass energy of 18 GeV, the highest energy achieved in fixed target ex-

periments [1]. The phenomenon of rising total cross sections is familiar in hadron–hadron collisions, where the measurements extend up to energies of 1.8 TeV. Depending on the specific model of high energy photon–proton collisions, the total cross section is predicted to lie in the range from 145 μb to 760 μb at 200 GeV [2]. In this letter we report an initial measurement of $\sigma_{tot}(\gamma p)$ in the centre of mass energy range 186 GeV to 233 GeV [3]. This measurement has been made with the ZEUS detector at the electron–proton collider HERA at DESY.

2. The method

Neutral current ep interactions are described by the exchange of a neutral gauge vector boson with $q^2 = -Q^2$, where q^2 is the square of the momentum transfer between the initial and final state electron. If the scattering angle of the final state electron is small, Q^2 is small and the exchanged particle is an almost real photon. In this way, ep reactions at very small Q^2 can be used to measure the photoproduction cross section. The observed ep cross section is related to that for γp by the formula

$$\frac{d^2\sigma(ep)}{dy\,dQ^2} = \frac{\alpha}{2\pi}\frac{1}{Q^2}\left(\frac{1+(1-y)^2}{y}\sigma_T(y,Q^2)\right.$$
$$\left. +2(1-y)\sigma_L(y,Q^2)\right), \qquad (1)$$

where, for small scattering angles, $y = (E_e - E'_e)/E_e$. E_e and E'_e are the energies of the incoming and outgoing electron in the laboratory frame, and σ_T and σ_L are the γp cross sections for transversely and longitudinally polarized virtual photons, respectively.

The acceptance of the apparatus confines our study to outgoing electrons whose energies and scattering angles correspond to a mean Q^2 of 6×10^{-4} GeV^2. It has been shown [4,5] that for such low Q^2, σ_L can be neglected and $\sigma_T(y,Q^2) \simeq \sigma_T(y)$. Integrating over the Q^2 range from $Q^2_{min} = m_e^2 y^2 E_e/E'_e$ to $Q^2_{max} \approx 2 \times 10^{-2}$ GeV^2, we obtained with these assumptions

$$\frac{d\sigma(ep)}{dy} = \frac{\alpha}{2\pi}\frac{1+(1-y)^2}{y}\sigma_T(y)\ln\frac{Q^2_{max}(y)}{Q^2_{min}(y)}. \qquad (2)$$

Finally we assume that in the limited range of scattered electron energies used for this study, the total

photoproduction cross section is energy independent, and use $\sigma_T(y) \simeq \sigma_{tot}(\gamma p)$:

$$\sigma(ep) = \frac{\alpha}{2\pi}\sigma_{tot}(\gamma p)$$
$$\times \int_{y_{min}}^{y_{max}}\left(\frac{1+(1-y)^2}{y}\ln\frac{Q^2_{max}(y)}{Q^2_{min}(y)}\right)\,dy. \qquad (3)$$

Thus by measuring the total ep cross section in a given y interval, one obtains the total γp cross section. The integration must also take account of the apparatus acceptance. The centre of mass energy of the γp system is $W = \sqrt{s} = 2\sqrt{yE_e E_p}$.

3. HERA operation

During its first running period, HERA operated with 26.6 GeV electrons and 820 GeV protons. Typical beam currents were 1–2 mA for each beam and were measured with inductive coils. Ten electron bunches collided with ten proton bunches. The time interval between consecutive bunches was 96 ns. An additional electron bunch, the pilot bunch, did not collide with a proton bunch, but was used for background studies. Since the electron bunches were much shorter in length than the proton bunches, the length of the interaction region was defined by the proton bunch length, and was typically ± 20 cm around the interaction point.

4. The experimental setup

The ZEUS detector is shown in fig. 1. Charged particles are tracked by the inner tracking detector system, comprising a vertex detector, a central tracking detector (consisting of cylindrical drift chamber layers), planar drift chambers in the forward and rear directions, and transition radiation detectors in the forward direction. Of these, only the central drift chamber was read out in the present running. In this work, we define the forward and rear directions to be those of the proton and electron beams, respectively.

A thin superconducting solenoid surrounding the inner tracking detector produces a magnetic field of
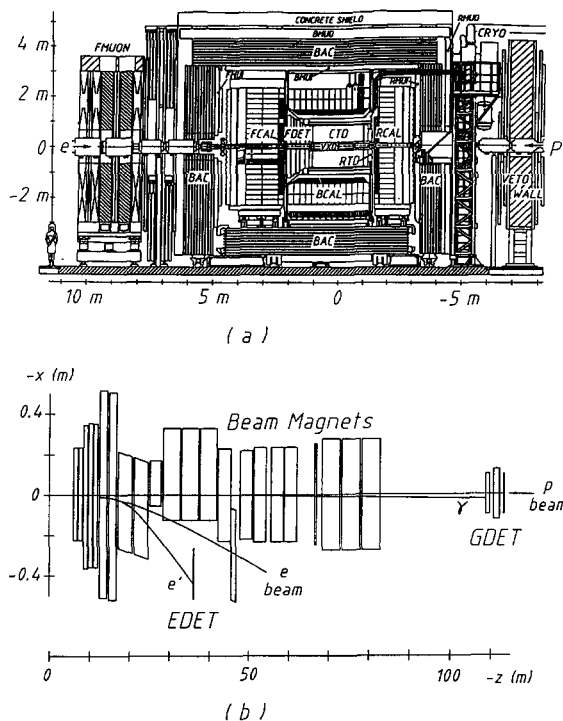
Fig. 1. The ZEUS apparatus: (a) side view, (b) top view of the luminosity monitor in relation to the interaction point ($x = z = 0$) and the electron and proton beamlines. GDET and EDET refer to the photon and scattered electron (e') detectors in the luminosity monitor; GDET and the proton beam line are vertically separated. Other parts of the apparatus are described in the text.

1.43 T in the centre. A uranium-scintillator calorimeter encloses hermetically the solenoid and inner tracking detectors. The magnetized iron yoke surrounding the calorimeter is instrumented for use as a backing calorimeter and muon detector. In the forward direction, iron toroids and tracking chambers reinforce muon detection. Downstream of the main detector in the proton direction, six measuring stations are installed in the proton ring for detecting forward scattered protons. Close to the beamline upstream of the main detector, photon and electron detectors are installed to measure the luminosity and to detect small angle electrons.

A set of scintillation counters (C5) partially surrounds the beam pipe behind the rear part of the calorimeter. This serves as a monitor of the timing of both beams and detects background events generated upstream of the detector by the proton beam.

The components used for the present measurement are the luminosity monitor, the uranium calorimeter, the central tracking detector, and the C5 counters.

4.1. The luminosity monitor

For the luminosity measurement, the bremsstrahlung process ep → e'γp is used, because it has a large and precisely known cross section. Its experimental signature is a coincidence of a photon and an electron at small angles to the electron beam direction, with energies adding up to the beam energy: $E'_e + E_\gamma = E_e$.

The ZEUS luminosity monitor [6] consists of a photon and an electron branch each equipped with lead-scintillator electromagnetic calorimeters (fig. 1b). Photons emerging from electron-proton interactions at angles $\theta_\gamma \leqslant 0.5$ mrad with respect to the beam axis leave the proton beam pipe at a distance of 92.5 m from the interaction point (IP) and hit the photon calorimeter (GDET) at 107 m from the IP. In front of the photon calorimeter, a two radiation length ($2X_0$) carbon filter is installed to absorb the large flux of synchrotron radiation photons. An air filled threshold Čerenkov counter is placed between the filter and the photon calorimeter to tag events in which a photon has converted in the carbon filter. Inside the calorimeter, at a depth of 7 X_0, a position detector made of scintillator fingers measures the horizontal and vertical position of the photon with an accuracy of about 2 mm.

Electrons scattered at angles $\theta'_e \leqslant 6$ mrad with respect to the beam axis, and with energies $0.2E_e < E'_e < 0.9E_e$, are deflected by beam magnets away from the electron beam orbit. They leave the electron beam pipe through a steel window at a distance of 27.3 m from the IP and hit the electron calorimeter (EDET) at 34.7 m from the IP.

A background arises from the bremsstrahlung of beam electrons on the residual gas in the beam pipe. It has the same signature as the main process and a similar differential cross section. The subtraction of this background is done by measuring the bremsstrahlung rate from the pilot electron bunch (R_{pilot}). If the current in the pilot bunch is I_{pilot} and the total current is I_{tot} then

$$R_{ep} = R_{tot} - R_{pilot} \cdot \frac{I_{tot}}{I_{pilot}}, \qquad (4)$$

where R_{ep} is the electron proton bremsstrahlung rate, and R_{tot} the total measured rate. In addition to the rates, data from a fraction of the luminosity events are continuously recorded to monitor the calibration of the calorimeters, the efficiency of the Čerenkov veto, the geometrical acceptance and the background conditions. The geometrical acceptance for the bremsstrahlung photons is about 98%, independent of the photon energy, and is measured using the position detector. The acceptance for the bremsstrahlung electrons is measured to be above 70% for the electrons with energies in the range $0.35E_e < E'_e < 0.65E_e$. For the luminosity determination we count the rate of electrons with these energies, in coincidence with high energy photons which did not convert in the carbon filter. Typical rates of 50–100 Hz were obtained during the running period.

For photoproduction, the electron calorimeter tags events in the Q^2 range from 10^{-7} to 2×10^{-2} GeV^2.

4.2. The calorimeter

The calorimeter [7] consists of plates of depleted uranium interleaved with plastic scintillator. The three sections of the calorimeter (Forward, Barrel and Rear) are shown as FCAL, BCAL and RCAL in fig. 1a. Their thicknesses are 7.1, 5.3 and 4 absorption lengths, respectively. The calorimeter is segmented longitudinally into an electromagnetic section (EMC) and two (one) hadronic sections (HAC) in FCAL, BCAL (RCAL). The scintillator tiles form cells, which are read out via wavelength shifter bars, light guides, and photomultipliers. Typical transverse cell sizes are 5 cm × 20 cm (10 × 20) in the FCAL, BCAL (RCAL) EMC sections, and 20 cm × 20 cm in all the HAC sections. There are 20 cm × 20 cm holes in FCAL and RCAL for the beam pipe. The active area of FCAL (RCAL) starts at 45 (68) mrad relative to the beam direction. The solid angle coverage is 99.8% in the forward hemisphere and 99.5% in the rear hemisphere. The calorimeter is compensating, giving equal response to hadrons and electrons. Under test beam conditions without material in front of the calorimeter, the energy resolution for electrons was $\sigma(E)/E = 0.18/\sqrt{E} \oplus 1\%$ (E in GeV, $\oplus$ stands for addition in quadrature) and for hadrons was $\sigma(E)/E = 0.35/\sqrt{E} \oplus 2\%$ [7,8]. In the off-line reconstruction, cells were ignored which had energy

less than 60 MeV in the EMC sections, or 100 MeV in the HAC sections.

The signals from the photomultipliers are used to provide fast timing information. The average times t_F and t_R for signals in the FCAL and RCAL cells are measured to typically 1 ns accuracy by using cells with energy greater than 1 GeV. The time $t=0$ for each of the cells is defined as the average time at which particles emitted at the IP reach the cell.

4.3. The central tracking detector

The central tracking detector (CTD) [9] consists of 72 cylindrical drift chamber layers organized into 9 'superlayers'. Four of these superlayers (2, 4, 6 and 8) have small stereo angles to allow the three dimensional reconstruction of tracks. All wires will have 100 MHz FADCs to allow accurate reconstruction in the r–ϕ plane. The three innermost axial superlayers (1, 3 and 5) are in addition instrumented with z-by-timing electronics [10], which measures the z coordinate from the difference in the time of arrival of pulses at each end of the wire. It also measures the r–ϕ coordinate from the arrival time of the pulse at the wire relative to the beam crossing time (in intervals of 48 ns). In this data taking period only the z-by-timing electronics was used. The present resolution in multitrack events is measured to be about 4.5 cm in z and 1 mm in r–ϕ.

4.4. The trigger

For normal data taking, the trigger was optimized for deep inelastic scattering (DIS) and had only $\approx$4% acceptance for photoproduction events. Special photoproduction runs were therefore taken using substantially lower energy thresholds than the DIS trigger. The photoproduction trigger required an electron with energy above 1.5 GeV in the luminosity monitor, together with an energy signal above threshold in at least one trigger tower in the calorimeter. The trigger towers are groups of calorimeter cells, of typical transverse size 20 cm×40 cm. The thresholds for cells within 30 cm horizontally and vertically from the beamline were 10 GeV for the FCAL and RCAL HAC trigger towers, and 10 GeV and 2.5 GeV for the FCAL and RCAL EMC trigger towers, respectively. Away from the beam the thresholds were: 5 GeV for FCAL HAC

and EMC, 5 GeV for RCAL HAC and 2.5 GeV for
RCAL EMC, and 1 GeV for BCAL HAC and EMC.
Events with a signal from the C5 counters in time with
the proton beam were rejected as proton beam associ-
ated background. The trigger tower efficiency above
threshold was >99%. Of the trigger towers, 3% were
non-functioning (but none near the beam); this had
a negligible effect in the present measurement.

4.5. The data selection

Data were taken using the photoproduction trigger
over a period of 7 hours of running, yielding an in-
tegrated luminosity of 227 μb^{-1} and 53212 recorded
events. These were passed through the standard ZEUS
reconstruction program.

The main signature for an event to be accepted as
a photoproduction candidate is a signal in the elec-
tron tagger (EDET) in the energy range 5–25 GeV, in
coincidence with energy in the uranium calorimeter.
A maximum energy of 0.5 GeV was permitted in the
photon detector of the luminosity monitor.

A major source of background comes from random
coincidences between a bremsstrahlung event and a
proton beam gas or beam wall event. This background
can be substantially reduced by using the timing in-
formation from the calorimeter, since particles gen-
erated upstream of the detector reach RCAL ≈ 12 ns
earlier than those emitted from the IP. Fig. 2a shows
a plot of $t_F - t_R$ versus t_R, demonstrating a clear sep-
aration between the background events and the pho-
toproduction candidates. A cut of $| t_F - t_R | < 5$ ns,
$| t_R | < 5$ ns, was imposed.

The above cuts still leave random coincidences be-
tween bremsstrahlung events and background events
originating in the detector region. These events were
rejected by demanding a minimum deposit of 1.1 GeV
in RCAL. Monte Carlo studies show that photopro-
duction events which are accepted by the trigger will
almost always deposit at least 1.1 GeV in RCAL. The
background events deposit less than 1 GeV.

To summarize, the selection criteria applied to the
photoproduction candidate sample are:
- $5 < E'_e < 25$ GeV, $E_\gamma < 0.5$ GeV,
- $| t_F - t_R | < 5$ ns, $| t_R | < 5$ ns,
- $E_{RCAL} > 1.1$ GeV.

The 212 events which satisfied these conditions were
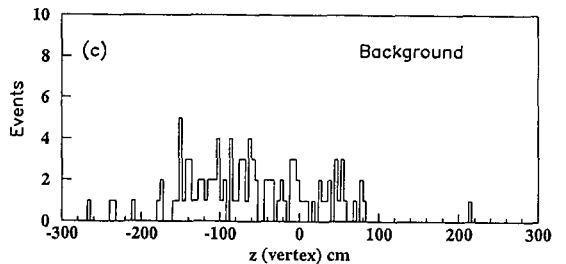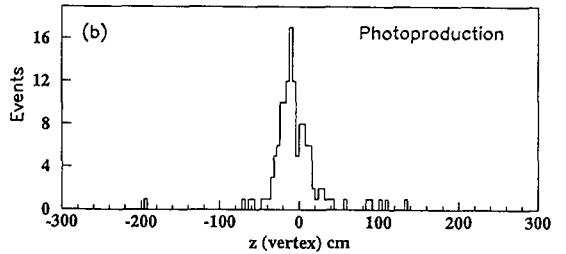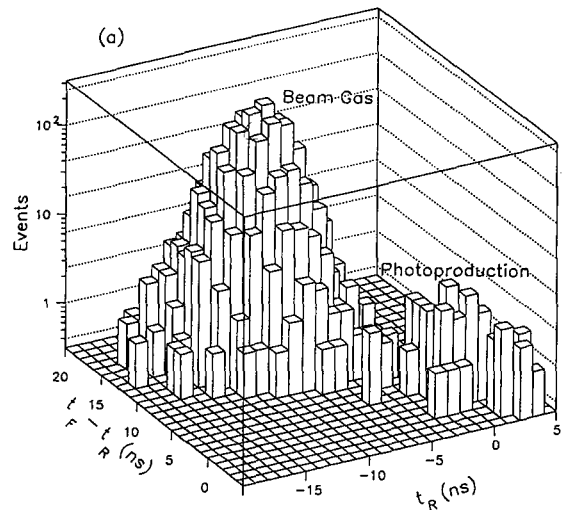scanned by at least two physicists to remove a contam-

Fig. 2. (a) Plot of the time difference between FCAL and
RCAL signals, $t_F - t_R$, versus the RCAL time, t_R. (b) Plot of
the reconstructed vertex for photoproduction candidates and
(c) background events having a bremsstrahlung signature
in the luminosity monitor. The vertex was calculated by
demanding at least two well reconstructed tracks in the CTD.

ination of cosmic ray events, and 182 events were ac-
cepted as photoproduction candidates. Vertices were
calculated for all events with at least two well recon-
structed tracks in the central tracking detector [11];
72% of the photoproduction candidates fell into this

473

category. Their vertex positions were found to peak close to the origin, in contrast to the uniform distribution in z characteristic of beam gas events (figs. 2b, 2c). Beam gas events were selected by requiring a random coincidence between a bremsstrahlung event detected in the luminosity monitor, together with an event with at least two reconstructed tracks in the central tracking detector.

The remaining background in this event sample comes mainly from electron gas scattering. It has been estimated by using data from a dedicated run with only the electron beam, and passing the events through the whole analysis procedure. Only one event survived. Furthermore, no event in the final sample was from the electron pilot bunch. The electron gas background was found to be less than 5% and has been neglected.

4.6. Acceptance calculation

For calculating acceptances, the existing generators PYTHIA [12] and HERWIG [13] were adapted to photoproduction. The scattered electron was generated according to the ALLM [4] prescription, which provides a smooth description of the transition from photoproduction to deep inelastic scattering. The 'elastic' channel $\gamma p \rightarrow \rho^0 p$ was incorporated by using standard ρ^0 parameters and an s-channel helicity conserving decay. The slope of the t distribution was taken as 10 GeV^{-2} [14]. The channel $\gamma p \rightarrow \gamma p$ can be neglected [14]. The inelastic diffractive reactions were generated according to the behaviour measured for photoproduction at lower energies [15]. For invariant masses of the diffractive system $M_X > 2$ GeV, a $1/M_X^2$ dependence was assumed, with a t slope of 5 GeV^{-2}. The generated events were processed through the standard programs for detector and trigger simulation and event reconstruction.

The acceptance of the electron tagger for photoproduction events has a broad maximum of about 60% in the energy range 10–16 GeV, independent of the details of the photoproduction process. For the calculation of the total γp cross section we have used only the 97 events with a scattered electron in this energy range (fig. 3a).

The acceptance of the main detector is process dependent. Using PYTHIA and HERWIG, we have generated the following six subprocesses: low p_T reac-
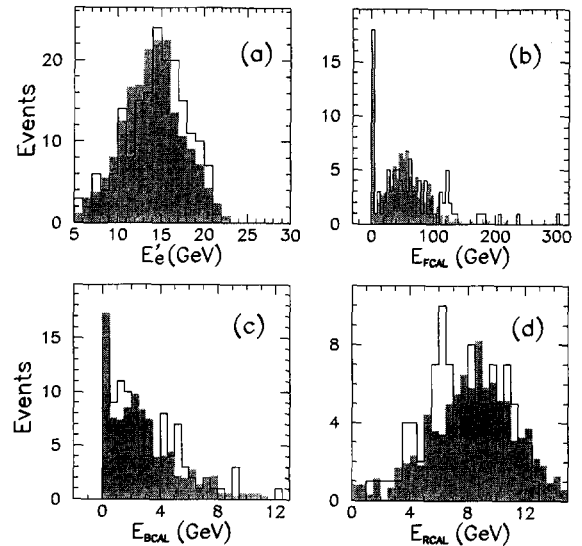

Fig. 3. (a) The energy of the scattered electron as measured by the tagger (EDET), for photoproduction events. (b)–(d) The energy deposited in FCAL, BCAL, and RCAL, respectively, for photoproduction events for which the scattered electron energy is in the range 10–16 GeV. The shaded distributions are the predictions from the Monte Carlo.

tions, elastic scattering (as defined above), single and double inelastic diffraction, and direct photon and resolved photon hard interactions (requiring transverse momenta of greater than 1 GeV/c in the hard scattering system). The acceptance for elastic events varied between 0.10–0.27, depending on the details of the model used. The acceptance for single and double inelastic diffractive events was 0.40 and 0.50, respectively, that for low p_T reactions was 0.70, and for the hard subprocesses the acceptance was 0.80. The values obtained from PYTHIA and HERWIG were similar.

The energy measured in the different parts of the calorimeter is displayed in figs. 3b–3d. The shaded distributions are the predictions of PYTHIA, using a mixture of 20% diffractive (including an elastic contribution) and 80% low p_T photoproduction events which were passed through the same analysis as the data. The agreement is satisfactory. The distributions obtained from HERWIG give similarly good agreement with the data. There are 18 events which deposit almost no energy in FCAL (fig. 3b). These are most likely either elastic or inelastic diffractive events

where no fragments are detected in FCAL. The fact that the Monte Carlo prediction is in agreement with this observation adds to the confidence in the assumed relative abundances for these processes and therefore in the computation of the acceptance. We have investigated the effect of varying the parameter governing the p_T of jet fragmentation in PYTHIA, in the range of ± 200 MeV/c about its nominal value of 350 MeV/c. This changed the acceptance for low p_T events between 0.54 and 0.79. We consider this to represent a safe estimate of our uncertainty of the acceptance for soft processes.

Within limits constrained by the fraction of events with no FCAL energy, we have varied the fraction of single diffractive events (including elastic) between 0.20 and 0.40 of the total [14,16,17], and have also investigated the effect of including admixtures of the hard processes. Since the acceptance of the latter is close to the central value of 0.70 used for the low p_T process, their inclusion does not affect the overall acceptance significantly. Overall main detector trigger acceptances varying in the range 0.49–0.68 were obtained. This spread is lower than that obtained for the low p_T process alone because the data require a higher (lower) fraction of low p_T events with lower (higher) acceptance. For the cross section calculation, a figure of 0.59 ± 0.09 was used.

5. Results

The scattered electron energy range $E'_e = 10$–16 GeV corresponds to a γp centre of mass energy range of $186 < \sqrt{s} < 233$ GeV. Using the average combined acceptance for the main detector and the electron tagger of 0.37, and the measured integrated luminosity, we obtain the cross section:

$$\sigma_{tot}(\gamma p) = 154 \pm 16 \ \mu b, \qquad (5)$$

where the error is statistical only and radiative corrections are not included.

In order to check the sensitivity of this result to the trigger thresholds and the details of the simulation, we have performed the following checks: (1) The trigger thresholds in the calorimeter were increased by 40% in the off-line analysis. This reduced the data sample to 64 events, and resulted in a cross section of $\sigma_{tot}(\gamma p) =$

$143 \pm 17 \ \mu b$. (2) The cross section was calculated using data from runs with the DIS trigger. The DIS trigger thresholds give an acceptance for photoproduction events which is about 10 times smaller than that for the photoproduction trigger. The 23 events from this sample give a cross section of $\sigma_{tot}(\gamma p) = 161 \pm 34 \ \mu b$. All errors quoted in these checks are statistical only.

5.1. Radiative corrections

The measured cross section may be affected by radiative processes of the type ep $\rightarrow$ e$'\gamma$X. In order to obtain the Born cross section one needs to apply radiative corrections to the measured data in the specific experimental situation. We studied these effects with two different programs. One uses an analytical approach (TERAD [18]) and the other is based on Monte Carlo techniques (HERACLES [19]). These programs were originally written for the deep inelastic region, and have been modified for the photoproduction region where, because of the low Q^2 values involved, the quark parton model interpretation is unreliable and the electron mass cannot be neglected.

Although the radiative corrections can be quite appreciable for certain y and Q^2 values calculated from the final state electron, they become small when the experimental conditions are included. There are two particular factors which reduce the corrections: the $E_\gamma < 0.5$ GeV cut in the angular acceptance region of the photon detector of the luminosity system, and the cut $E_{RCAL} > 1.1$ GeV. This latter cut puts a minimum value of 60 GeV on the centre of mass energy of the hadronic system. The resulting radiative corrections by both TERAD and HERACLES are about 1%, and have therefore been neglected. The number of radiative events rejected by the selection criteria was consistent with these estimates.

5.2. Systematic errors

The principal sources of systematic error in this measurement are the uncertainties on the luminosity, the trigger acceptance of the main detector and the acceptance of the electron tagger.

The main effects which contribute to the systematic error of the luminosity determination are the subtraction of the beam gas background, the effect of the carbon filter, background in the Čerenkov counter and

the geometrical acceptance. Test runs have been taken to study these effects. At the present state of analysis we estimate an 11% overall uncertainty, which is expected to be reduced by further investigations.

The fractional systematic error on the acceptance of the electron tagger is 10% and that of the acceptance of the main detector is 15%. Adding all systematic errors quadratically, the total systematic error is 21%. We thus quote the total photoproduction cross section at an average centre of mass energy of 210 GeV as

$$\sigma_{tot}(\gamma p) = 154 \pm 16 \text{ (stat.)} \pm 32 \text{ (syst.)} \ \mu b. \qquad (6)$$

6. Discussion of the result

There exist various predictions for the value of the total photoproduction cross section at high energies. These are based either on a phenomenological Regge-type approach [20,4], or on perturbative QCD [21–25]. The predictions of the latter models depend on the parton parametrizations of the proton and the photon. They also depend on the value of p_T^{min}, which is the lower limit of the integration of the part of the cross section coming from hard interactions, which is added to the soft cross section.

Fig. 4 shows the total photoproduction cross section as a function of the γp centre of mass energy W. It includes the lower energy measurements above the resonance region ($W > 1.75$ GeV) [26], together with the result of this experiment. The error shown includes the 10% statistical error added linearly to the 21% systematic error. The two solid curves, labelled DL [20] and ALLM [4], are Regge-type analyses which have used the lower energy photoproduction measurements, together with proton structure function data, to predict the behaviour of the total γp cross section at higher energies. The other four curves are predictions based on the assumption that the total cross section is the sum of a soft and a hard part, using the eikonal formalism [2]. All four use the KMRS [27] parametrization for the parton distribution in the proton. The dotted curve uses the LAC1 [28] parametrization for the parton distributions in the photon taking $p_T^{min} = 1.4$ GeV/c. The dashed curve is the same with a $p_T^{min} = 2$ GeV/c. The two dash–dotted curves use the DG [29] parametrization for parton distributions in the pho-

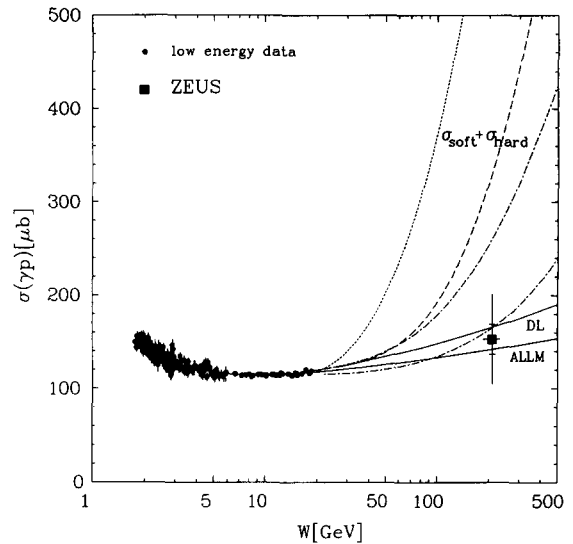Fig. 4. The total γp cross section measurements at low energies (full circles) together with that measured by ZEUS at HERA (full square). The lower solid curve is the prediction of the ALLM parametrization and the higher solid curve is that of DL. The dotted (dashed) line uses the LAC1 parametrization for the photon with $p_T^{min} = 1.4$ GeV/c (2 GeV/c). The dash–dotted lines use the DG parametrization for the photon with $p_T^{min} = 1.4$ GeV/c (upper line) and $p_T^{min} = 2.0$ GeV/c (lower).

ton, taking $p_T^{min} = 1.4$ GeV/c (upper curve) and $p_T^{min} = 2.0$ GeV/c (lower). Our measurement favours the lower theoretical predictions.

References

[1] D.O. Caldwell et al., Phys. Rev. Lett. 40 (1978) 1222.

[2] See G.A. Schuler, Proc. Workshop on Physics at HERA (DESY, Hamburg, 1992) p. 461;
A. Levy, Proc. Workshop on Physics at HERA (DESY, Hamburg, 1992) p. 481.

[3] Preliminary results for this cross section were reported by the two HERA experiments, H1 and ZEUS, at the 26th Intern. Conf. on HEP (Dallas, August 1992).

[4] H. Abramowicz, E.M. Levin, A. Levy and U. Maor, Phys. Lett. B 269 (1991) 465.

[5] A.I.Lebedev, Proc. Workshop on Physics at HERA (DESY, Hamburg, 1992) p. 613.

[6] J. Andruszków et al., DESY 92-066 (1992).

[7] M. Derrick et al., Nucl. Instrum. Methods A 309 (1991) 77;
A. Andresen et al., Nucl. Instrum. Methods A 309 (1991) 101.

[8] A. Bernstein et al., to be submitted to Nucl. Instrum. Methods (1992);
U. Mallik, Proc. Intern. Conf. on High energy physics (FNAL, Batavia, IL, 1990).

[9] C.B. Brooks et al., Nucl. Instrum. Methods A 283 (1989) 477.

[10] N. Harnew et al., Nucl. Instrum. Methods A 279 (1989) 290;
B. Foster et al., Proc. 3rd Intern. Conf. on Advanced technology and particle physics (Villa Omo, Como, 1992), Oxford University preprint OUNP - 92 - 14, Nucl. Instrum. Methods, to be published.

[11] P.Billoir and S.Qian, Nucl. Instrum. Methods A 311 (1992) 139.

[12] T. Sjöstrand, Z. Phys. C 42 (1989) 301.

[13] B.R. Webber, Ann. Rev. Nucl. Part. Sci. 36 (1986) 253.

[14] T.H. Bauer et al., Rev. Mod. Phys. 50 (1978) 261.

[15] T.J. Chapin et al., Phys. Rev. D 31 (1985) 17.

[16] K. Goulianos, Phys. Rep. 101 (1983) 169.

[17] L. Caneschi, G. Delfino, Phys. Lett. B 253 (1991) 265.

[18] A. Akhundov et al., Proc. Workshop on Physics at HERA (DESY, Hamburg, 1992) p. 1285.

[19] A. Kwiatkowski, H. Spiesberger and H.-J. Möhring, Proc. Workshop on Physics at HERA (DESY, Hamburg, 1992) p. 1294.

[20] A. Donnachie and P.V. Landshoff, Nucl. Phys. B 231 (1984) 189.

[21] G. Schuler and J. Terron, CERN-TH.6415/92 (1992).

[22] M. Drees and F. Halzen, Phys. Rev. Lett. 61 (1988) 275.

[23] R. Gandhi and I. Sarcevic, Phys. Rev. D 44 (1991) R10.

[24] J.R. Forshaw and J.K. Storrow, Phys. Lett. B 268 (1991) 116.

[25] J.C. Collins and G.A. Ladinsky, Phys. Rev. D 43 (1991) 2847.

[26] S.I.Alekhin et al., CERN-HERA 87-01 (1987).

[27] J. Kwiecinski, A.D. Martin, W.J. Stirling and R.G. Roberts, Phys. Rev. D 42 (1990) 3645.

[28] H. Abramowicz, K. Charchuła and A. Levy, Phys. Lett. B 269 (1991) 458.

[29] M. Drees and K. Grassie, Z. Phys. C 28 (1985) 451.